Sensors and Materials, Vol. 10, No. 3 (1998) 155–168
MYU Tokyo

S & M 0321

A Tunable Optomechanical Micromirror Switch

Kyoung-Sun Seo, Young-Ho Cho and Sung-Kie Youn

Department of Mechanical Engineering
Korea Advanced Institute of Science and Technology
373-1 Yusong-ku, Kusong-dong, Taejon 305-701, Korea

(Received April 2, 1997; accepted February 4, 1998)

Key words: micromirror, optomechanical switch, frequency tuning, electrostatic actuation, bulk-micromachining

The paper presents the electromechanical analysis, design, fabrication and characterization of a bulk-micromachined electrostatic micromirror device, whose optomechanical switching frequency is electrically tunable after fabrication. The silicon micromirror, fabricated via anisotropic etching of (110) silicon wafers, was suspended by two pairs of boron-diffused microflexures. The optical switching function was obtained by an electrostatic translational motion of the micromirror in the direction parallel to the substrate. In a static performance test, stable translational motion of the micromirror was observed up to the threshold deflection of 26.5 μm at the DC threshold voltage of 330 V. In dynamic operation, resonant switching frequencies were electrically tuned in the range of 585–450 Hz using the DC bias voltage in the range of 50–300 V for an AC drive voltage of 10 V.

1. Introduction

Recently, micromachined mirrors[1–5] have been receiving increasing attention for applications to optomechanical switching devices. Among them, surface-micromachined torsional micromirrors,[1–4] suspended parallel to the silicon substrates, modulate optical signals normal to the substrates. The maximum size of surface-micromachined mirrors, however, is constrained due to adhesion problems[6] as well as etch selectivity, defined as the width-to-thickness ratio of the sacrificial layer to be etched underneath the structural layer. For laser beam and optical fiber applications, we need mirrors that are hundreds of micrometers in size, which requires special sacrificial layer materials or holes being produced on the mirror surfaces for surface-micromachined mirrors.

In this paper, we present a bulk-micromachined translational micromirror device (Fig. 1) for optical switch applications. A high-aspect-ratio micromirror with high-quality (111) crystalline surfaces[5] has been fabricated by anisotropic etching of (110) silicon[5,7] having height and width of the order of hundreds of micrometer. The bulk-micromachined mirror, suspended normal to the substrate, modulates the optical signals on the plane parallel to the substrate. The previous bulk-micromachined device[5] utilized an electrostatic "bending" motion of the silicon strip, whose (111) sidewalls act as mirror surfaces. The present device shown in Fig. 1, however, utilizes an electrostatic "translational" motion of the solid silicon micromirror, suspended by two pairs of thin microflexures. Compared to the bending mirror, the translational mirror provides more accurate prediction of the location and direction of reflected beams.

This paper describes the design, fabrication and testing of the translational switching micromirror with an emphasis on the post-fabrication tuning of the switching frequency. The static switching function is tested using an electrostatic translational drive of the micromirror in the direction parallel to the substrate. A dynamic switching function has been achieved by the resonant translational motion of the micromirror, driven by an AC drive voltage with a DC bias voltage. In the dynamic performance test, the switching frequency and the amplitude of the resonant micromirror are adjusted by the DC bias voltage and the AC drive voltage, respectively.

2. Electromechanical Analysis and Design

Figure 1 shows a perspective view of the switching micromirror device, whose resonant-switching frequency is tunable after fabrication. The electrostatically driven

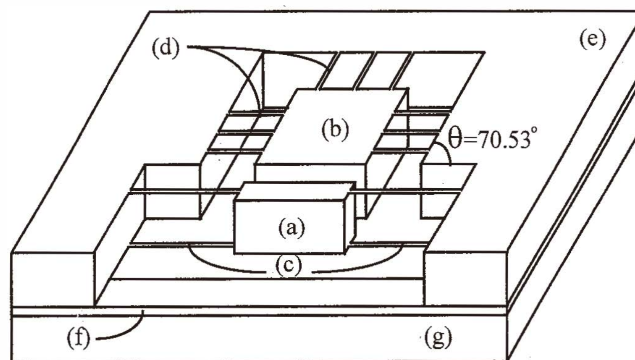

Fig. 1. Perspective view of the switching micromirror device: (a) micromirror; (b) counter electrode; (c) microflexures; (d) dummy supporting beams; (e) silicon body; (f) bonding layer; and (g) silicon base.

micromirror is suspended by two pairs of microflexures. For the translational switching motion of the micromirror, the microflexures act not only as mechanical flexural suspension, but also as electrical interconnection between the micromirror and electrode. The dummy supporting beams in Fig. 1 suspend the counter-electrode during the fabrication process. They are destroyed after the bonding of the fabricated devices and the silicon base; thus, the counter electrode is electrically isolated from the silicon body.

2.1 *Optical scan width*

Figure 2 illustrates the optical switching function of the micromirror device. The translational mirror motion, x, changes the path of the reflected signal. In Fig. 2, the scan width, s, is defined by the parallel displacement of the output optical signal due to the translational mirror motion, x as

$$s = 2x \sin\phi, \tag{1}$$

where ϕ is the incident angle of the optical signal.

2.2 *Electrostatic and spring forces and threshold conditions*

The electrostatic force, F_e, between the mirror and the counter electrode in Fig. 3 is expressed as

$$F_e = \frac{\varepsilon}{2} \frac{AV^2}{(d-x)^2 \sin\theta}, \tag{2}$$

where V is the interelectrode voltage, ε is the dielectric constant of air, $\theta = 70.53°$ is the angle between (111) crystalline planes perpendicular to the surface of the (110) silicon

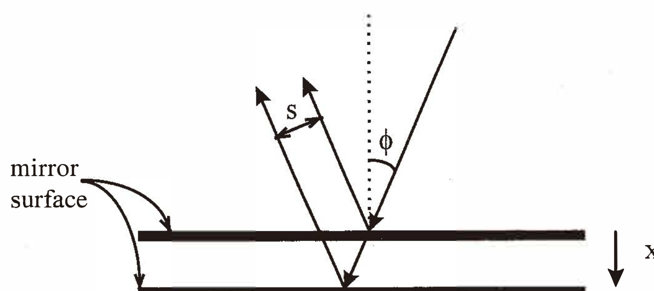

Fig. 2. Optical switching function of the translational micromirror motion; scan width, s, is obtained by the mirror deflection, x, for the incident angle, ϕ, of the optical input signal.

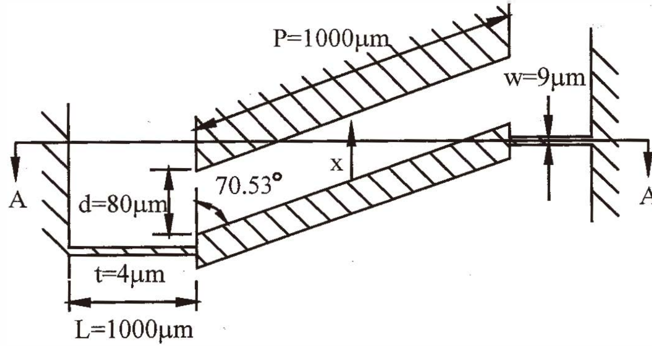

Fig. 3. Top view of the silicon micromirror and the counter electrode of Fig. 1.

substrate, A is the electrode area, d is the interelectrode distance and x is the deflection of the micromirror.

The spring force, F_s, generated by the beam deflection, x, is given[(8)] as

$$F_s = k_x x = \frac{48EI}{L^3}x, \tag{3}$$

where E is Young's modulus of microbeams, I is the second moment of inertia, L is the beam length and k_x is the spring constant of the microsuspension in the x-direction. From eqs. (2) and (3), we obtain the micromirror deflection, x, generated by the electrostatic voltage, V. In Fig. 4, it is noted that the electrostatic deflection, x, becomes unstable over the threshold condition, where the spring force line is tangential to the electrostatic force curve. Figure 4 illustrates that the threshold condition, defined by the threshold displacement, x_t, and the threshold voltage, V_t, is obtained at the point where the spring force line, tangential to the electrostatic force curve, coincides with the spring force obtained from eq. (3). At the threshold condition, the spring force line is obtained as

$$F = \frac{\varepsilon A V_t^2}{(d-x_t)^3 \sin\theta}(x - x_t) + \frac{\varepsilon A V_t^2}{2(d-x_t)^2 \sin\theta}. \tag{4}$$

From eqs. (3) and (4) we find that the threshold displacement of the micromirror, x_t, is equal to $d/3$. From the relation of $x_t = d/3$, we also obtain the beam stiffness and critical length at the threshold condition as

$$k_x = 48\frac{EI}{L^3} = \left(\frac{27}{8}\right)\left(\frac{\varepsilon A V_t^{\,2}}{d^3 \sin\theta}\right) \tag{5}$$

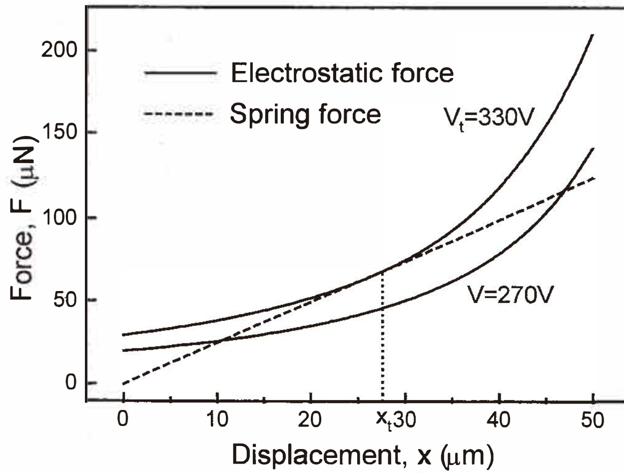

Fig. 4. Displacement-dependent electrostatic force and spring force: threshold condition, where the spring force line is tangential to the electrostatic force curve, is indicated by the deflection, x_t, and the electrostatic voltage, V_t.

$$L = \left(\frac{128}{9} \frac{EId^3 \sin\theta}{\varepsilon A V_t^2} \right)^{\frac{1}{3}}. \tag{6}$$

From eqs. (2), (3) and (5), the displacement, x, generated by the DC voltage of V between two parallel plate capacitors separated by a distance, d, can be obtained as:

$$\frac{x}{d}\left(1-\frac{x}{d}\right)^2 = \frac{4}{27}\left(\frac{V}{V_t}\right)^2. \tag{7}$$

2.3 *Resonant switching frequency*

For a zero DC bias voltage, $V_e = 0$, the resonant frequency of the micromirror, suspended by microflexures, is obtained as:

$$f = \frac{1}{2\pi}\sqrt{\frac{k_x}{m}}, \tag{8}$$

where m and k_x are the mass of the micromirror and the stiffness of the microflexures, respectively. For a DC bias voltage, V_e, the resonant frequency of the suspended micromirror is obtained as

$$f_e = \frac{1}{2\pi}\sqrt{\frac{k_e}{m}} \tag{9}$$

where the equivalent dynamic stiffness, k_e, is expressed as

$$k_e = k_x - \frac{\varepsilon A V_e^2}{\sin\theta (d - x_e)^3}, \tag{10}$$

where x_e represents the deflection of the micromirror generated by V_e. The first term in eq. (10) indicates the mechanical stiffness of the microflexures and the second term represents the effective stiffness[9] due to electrostatic forces. Since the electrostatic force due to the DC bias is proportional to the displacement, it act as an equivalent spring force in the dynamic equation of the micromirror motion. The electrostatic force generates an equivalent spring force in the direction opposite to the direction of the mechanical spring force, thereby reducing the net spring force. The electrostatic force due to the DC bias also generates tension in the beam. The resonant frequency change caused due to tension, however, is much less than that caused due to electrostatic forces. Therefore, the net effect of electrostatic force is a decrease in resonant frequency.

From eqs. (8) – (10), the resonant frequency, f_e, of the micromirror motion is expressed in terms of V_e and x_e as

$$f_e = f\left[1 - \frac{8}{27}\left(\frac{V_e}{V_t}\right)^2\left(\frac{d}{d - x_e}\right)^3\right]^{\frac{1}{2}}, \tag{11}$$

where f denotes the resonant frequency of the micromirror under zero interelectrode bias voltage, as defined by eq. (8). Equation (11) shows that the resonant frequency of the micromirror motion can be adjusted by the interelectrode bias voltage, since x_e is also a function of V_e.

2.4 *Squeeze film damping*

For the resonant motion of the micromirror, the air layer between the micromirror and the counter-electrode in Fig. 3 generates damping forces. The damping coefficient, C, is estimated [10] as

$$C = \frac{\mu A^2}{2}\left[\frac{1}{(d-x)^3} + \frac{1}{(d+x)^3}\right], \tag{12}$$

for the micromirror of the area, A, the air gap, d, and the dynamic vibration amplitude, x, where the viscosity $\mu = 1.82\times 10^{-5}$ N·s/m^2 for air at 20°C, 1 atm. For a small oscillation, $x \ll d$, eq. (12) is reduced to

$$C = \frac{\mu A^2}{d^3}. \tag{13}$$

The critical damping coefficient, C_c, for the micromirror device with the mass, m, and the suspension stiffness, k_{eq}, is obtained as

$$C_c = 2\sqrt{k_{eq} m}. \tag{14}$$

From eqs. (13) and (14), the damping ratio, ζ, of the micromirror device is found to be

$$\varsigma = \frac{C}{C_c} = \frac{\mu A^2}{2m(2\pi f_e)d^3} = \frac{\mu A}{4\pi\rho w f_e d^3}, \tag{15}$$

where ρ and w are the density and the thickness, respectively, of the micromirror. Near resonance, the quality factor of the micromirror device is defined as

$$Q = \frac{1}{2\varsigma}. \tag{16}$$

The damped resonant frequency, f_d, is then expressed as

$$f_d = f\sqrt{1-\varsigma^2}, \tag{17}$$

where the damping ratio, ζ, is defined by eq. (15).

3. Microfabrication

Figure 5 illustrates the microfabrication process for the switching micromirror device shown in Fig. 1. The process starts with the growth of 4000-Å-thick thermal oxide layers on both sides of a 400-μm-thick double-side-polished, p-type (110) silicon wafer.

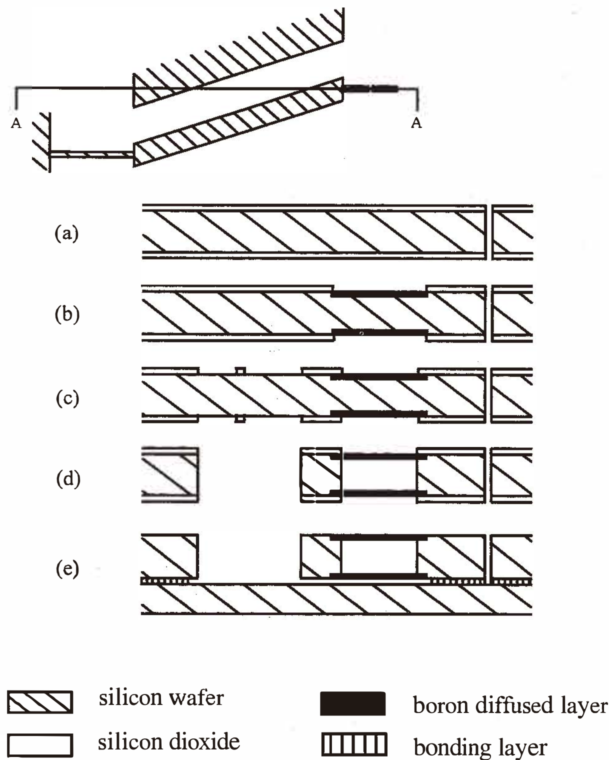

Fig. 5. Microfabrication process for the silicon micromirror device: A cross-sectional view along A-A of Fig. 2.

In the processing step shown in Fig. 5(a), an anisotropic EDP (Ethylene-Diamine Pyrocathechol water) etching process defines double-side alignment keys. Then the oxide layers are patterned to define diffusion masks. Figure 5(b) shows a 14-hour boron diffusion performed at 1100°C to define microflexures and dummy supporting beams. The boron diffusion depth of 4 μm has been designed for the microbeam thickness (Table 1). The oxide etching process shown in Fig. 5(c) defines etch masks for the micromirror and the counter electrode. Then the anisotropic silicon etching process of Fig. 5(d) defines the micromirror, the counter electrode and the boron-diffused microbeams, simultaneously.

In the silicon bulk-micromachining process shown in Fig. 5(d), we use EDP as the anisotropic silicon etchant and a thermally grown wet silicon dioxide as the etch mask. Since the boron-diffused layers are self-protected against the EDP solution, no other protection is required for the microbeam fabrication during the EDP bulk-micromachining.

For convex corner protection, we devised a new method and the associated structures, illustrated in Fig. 6. The corner compensation technique is based on the direction-dependent anisotropic silicon etch rates. As illustrated in Fig. 6, we use dummy dividers, whose widths are designed to be etched upon the etch-through of the substrate. The present corner protection technique has been effective in protecting convex corners during (110) silicon substrate etching, especially due to the simplicity and small size of the corner compensation structures.

In the final step shown in Fig. 5(e), we eliminated the dummy supporting beams after the bonding of the fabricated structure and the silicon base. We cut and placed a strip of thermoplastic tape between the silicon body of the mirror structure and the silicon base to bond the wafers together. Figure 7 shows the fabricated silicon microswitching device, where the high-aspect-ratio micromirror, 1000 μm long, 400 μm high and 90 μm thick, is suspended by two pairs of the microflexures, each being 1000 μm long, 9 μm wide and 4 μm thick. The boron-diffused dummy supporting beams are destroyed after the tape bonding of the fabricated device on the silicon base. In the bonding process, we use 100-μm-thick adhesive thermoplastic polymer tape, which allows bonding at the temperature of 300°C.

Table 1
Prototype of the switching micromirror device.

Parameter	Value
Flexure length (L)	1000 μm
Flexure thickness (t)	4 μm
Flexure width (w)	9 μm
Interelectrode distance (d)	80 μm
Interelectrode area (A)	1000 μm × 400 μm

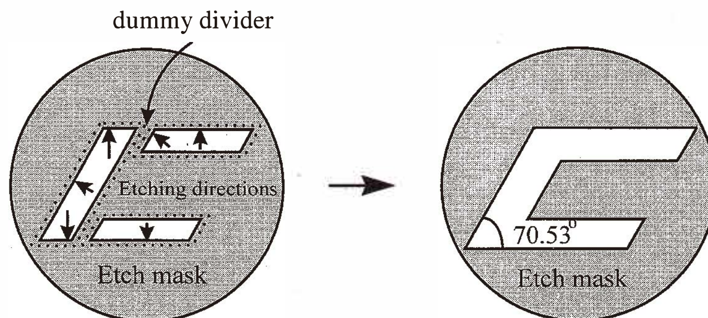

Fig. 6. Corner compensation technique using etch dividers.

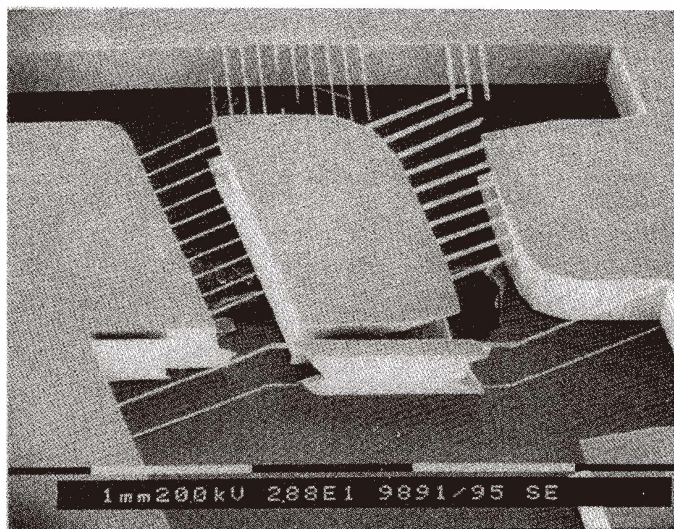

Fig. 7. SEM photograph of the fabricated switching micromirror device.

4. Experimental Results and Discussion

Static and dynamic switching tests were performed using the fabricated micromirror device. For the static switching test mirror deflection caused by an electrostatic DC voltage was measured. Figure 8 compares the measured deflections of the micromirror and the values estimated from eq. (7) using the measured V_t for varying electrostatic DC voltages. In the static drive test, stable deflection of the micromirror was observed up the threshold deflection of 26.5 μm at the threshold DC voltage of 330 V. For deflection over the threshold level, the deflection of the micromirror was suddenly increased so that the micromirror was attached to the counter electrode.

In a dynamic test, an AC drive voltage was applied with an electrostatic DC bias voltage. The resonant frequency was measured at the point at which the maximum amplitude of the micromirror was obtained during the frequency sweep of the AC drive voltage. The resonant frequency of the fabricated device was 590 Hz for a 10 V-amplitude AC drive voltage with zero bias voltage, where the visual resonance was observed at the AC driving frequency of 295 Hz. Therefore, the measured resonant frequency of 590 Hz at zero bias voltage corresponds to the mechanical resonant frequency, which is double the driving AC frequency at zero DC bias voltage. However, the resonant frequencies in Fig. 9 with non-zero bias voltage were measured using the AC drive voltage of 10 V with the DC bias voltage range of 50–350 V. The mechanical resonant frequency was obtained at the AC driving voltage frequency. Since the DC bias voltage is greater than the AC drive voltage, the actuation force with the half driving frequency is negligible. The actuation

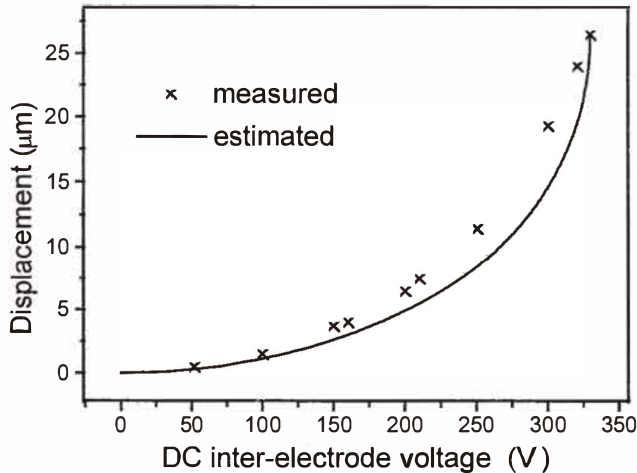

Fig. 8. Measured and estimated static displacement of the micromirror for varying DC interelectrode voltages.

with half frequency was observed only if the DC bias voltage was less than the AC drive voltage.

Table 2 shows the natural frequency of the fabricated structure, obtained from the finite element method (FEM) simulation. The measured resonant frequency was about 15% lower than the estimated value. From eqs. (12) to (16) we obtained the Q-factor of 11.26 for the microfabricated device. From eq. (17) we found that the air damping, neglected in the finite element analysis, caused less than 1% reduction of the resonant frequency, thus it was negligible source of discrepancy between the estimated and measured resonant frequencies. The major source of discrepancy seems to come from the errors in the material properties estimation, including the Young's modulus and residual stress, as well as errors in the size measurement. In the finite element analysis, we assumed Young's modulus of the boron-diffused silicon as 125 GPa[11] and neglected the residual stress. Due to the silicon etching errors, the effective width of the fabricated mirror was about 10% smaller than that of the designed value listed in Table 1.

For a 10 V-amplitude AC drive, resonant switching frequency of the fabricated device was tuned in the range of 585 – 450 Hz by adjusting the DC bias voltage in the range of 50 – 300 V. Figure 9 shows a comparison of the resonant frequencies measured from the fabricated device and those estimated from eq. (11) with the measured resonant frequency of 590 Hz. The errors in Fig. 9 come from the theoretical assumption of an infinite parallel plate capacitor embedded in eq. (11) and the spring stiffening effect neglected in eq. (10). In the dynamic operation of the micromirror, the threshold condition was not observed up to the maximum mirror amplitude of 80 μm. It was demonstrated that the switching or scanning frequency of the micromirror device can be adjusted by the DC bias voltage level,

Table 2
Dynamic performance of the switching micromirror, simulated by finite element analysis.

Mode # (Motion)	Resonant frequency
Mode 1 (Vertical)	289.1 Hz
Mode 2 (Horizonral)	686.6 Hz
Mode 3 (Torsional)	1160.8 Hz

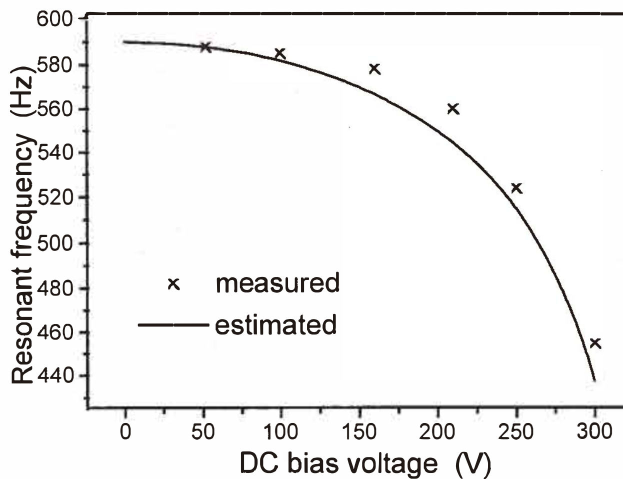

Fig. 9. Resonant switching frequencies of the micromirror, tuned using the DC bias voltage with a fixed AC drive voltage of 10 V.

while the switching amplitude or scanning width can be modified by adjusting AC drive voltage level.

5. Conclusions

We presented a bulk-micromachined single-crystal silicon micromirror, whose resonant switching-frequency and amplitude can be tuned by the adjustment of DC bias voltage and AC drive voltage, respectively. The translational micromirror, suspended by two pairs of boron-diffused micromechanical beams, was designed to be driven parallel to the silicon substrate for the optical switching function. The associated bulk-micromachining process, including a new corner compensation technique, was developed to obtain high-aspect-ratio micromirrors with (111) silicon surfaces. In the static performance test, a stable motion of

the micromirror was observed up to the threshold deflection of 26.5 μm at the measured threshold voltage of 330 V. In the dynamic switching test, the mechanical resonant frequency of the suspended micromirror was measured as 590 Hz with no bias voltage. The resonant frequency was tuned in the range of 585 – 450 Hz using the DC bias voltage adjusted in the range of 50 – 300 V. The present micromirror switching device is applicable to a variety of optomechanical microdevices, including optical shutters, scanners and couplers, as well as optical switches, whose resonant frequencies or amplitudes for the switching and scanning functions are required to be tuned or adjusted electrically after fabrication.

References

1 J. B. Sampsel: Tech. Digest of Solid-State Sensors and Actuators (1993) 24.
2 H. Toshiyosh and H. Fujita: Tech. Digest of Solid-State Sensors and Actuators (1995) 297.
3 V. P. Jaecklin, C. Linder and N. F. deRooij: Proc. IEEE Micro Electro Mechanical Systems Workshop, 1993, p. 124.
4 J. Buhler, J. Funk, O. Paul, F. P. Steiner and H. Baltes: Sensors and Actuators A **47** (1995) 572.
5 Y. Uenishi, M. Tsugai and M. Mehregany: J. Micromech. Microeng. **5** (1995) 305.
6 E. Bassous: IEEE Trans. Electron Devices **ED – 25** (1978) 1178.
7 C. H. Mastrangelo and C. H. Hsu: J. Microelectromech. **2** (1993) 33.
8 F. P. Beer and E. R. Johnston: Mechanics of Materials (McGraw-Hill, 1985).
9 K. B. Lee, J.-B. Yoon, M.-S. Kang, Y.-H. Cho, S.-K. Youn and C-K Kim: Proc. IEEE Conference on Emerging Technologies and Factory Automation, 1996, p. 498.
10 J. J. Blech: J. Lubrication Technology **105** (1983) 615.
11 J. S. Go, Y.-H. Cho, B. M. Kwak and K. Park: Sensors and Actuators A **54** (1996) 578.

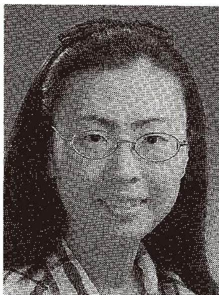

Kyoung-Sun Seo was born in Seoul, Korea, in 1971. She received the B.S. and M.S. degrees in Mechanical Engineering from the Korea Advanced Institute of Science and Technology (KAIST), Taejon, Korea, in 1994 and 1996, respectively. Currently, she is studying for a Ph.D. degree in MEMS area at KAIST. Her research interests include the micro-optoelectromechanical devices and integrated systems for information and communication applications.

Young-Ho Cho was born in Taegu, Korea, in 1957. He received the B.S. degree *summa cum laude* from Yeungnam University, Taegu, Korea, in 1980; the M.S. degree from KAIST, Seoul, Korea, in 1982; and the Ph.D. degree from the University of California at Berkeley (UCB) for his MEMS work completed in December, 1990. From 1982 to 1986 he was a Research Scientist of CAD/CAM Research Laboratory, Korea Institute of Science and Technology (KIST), Seoul, Korea. During 1987–1991, he worked as a Graduate Student Researcher (1987–1990) and a Post-doctoral Research Associate (1991) of the Berkeley Sensor and Actuator Center (BSAC) at UCB. In August 1991, Dr. Cho moved to KAIST, where he is currently an Assistant Professor in the Mechanical Engineering Department. He has served as the Chairman of the Steering Committee for Korea Government MEMS Program and the Technical Program Committee Member of IEEE MEMS Workshop. Dr. Cho's research interests are focused on the areas of functional micromechanical structures, microactuators, inertial microsensors, micro optoelectromechanical devices and systems. Dr. Cho is a member of IEEE and ASME.

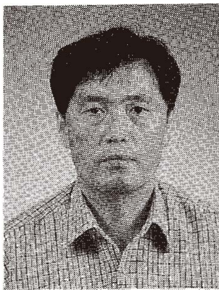

Sung-Kie Youn received the B.S. degree from the Seoul National University in 1975, and the M.S. and Ph.D. degrees in Engineering Mechanics from the University of Texas at Austin in 1983 and 1987, respectively. Subsequent to obtaining his Ph.D degree in 1987, he began working as a senior research engineer, at Computational Mechanics Co. in Austin, Texas, until he joined the faculty of Mechanical Engineering Department at KAIST, Korea, in 1988. Currently he is an Associate Professor at the department. His research topics includes finite element method for the coupled field problems, finite element analysis and parallel computation, homogenization method, topology and shape optimization of structural members, and analysis and constitutive modeling of rubber-like viscoelastic materials.